Extended Abstracts of the 2021 International Conference on Solid State Devices and Materials, VIRTUAL conference, 2021, pp39-40

Carrier Transport properties of Ferroelectric $Hf_{0.5}Zr_{0.5}O_2$ Thin Films in Poling Treatment

Yukinori Morita, Hiroyuki Ota, Shinji Migita

AIST
1-1-1, Umezono, Tsukuba, Ibaraki, 305-8568, Japan

Abstract

Carrier transport properties of ferroelectric $Hf_{0.5}Zr_{0.5}O_2$ (HZO) thin films are investigated on metal-ferroelectric-metal (MFM) capacitor in the first current flow of ferroelectric poling treatment. In current–voltage (*I–V*) measurement of MFM capacitor, a kink in *I–V* characteristic appears, and after the cyclic voltage sweep this kink disappears. From analysis using Poole-Frenkel plot of *I–V* characteristics, it is suggested that apparent dielectric constant of HZO abruptly changes in kink voltage in poling treatment.

1. Introduction

In recent increasing attentions to the IoT/AI system application of integrated circuit, power consumption reduction realized by novel computing frameworks such as in-memory or neural-networking computing will be a key for treating increasing information capability. HfO_2-based ferroelectric memory is one of the promising novel memories applicable for large-scale in-memory computing implementation.

One of the largest problems on HfO_2-based ferroelectric memory is endurance tolerance or so-called wake-up phenomena in cyclic write-erase operation. It has been reported that electric field driving polarization switch would affect redistribution of oxygen vacancy or crystallographic structures [1]. Before such cyclic operation, in general, poling treatment needs to be executed in ferroelectric material devices, which is first electric field driving operation.

In this paper we have focused on this poling treatment of ferroelectric capacitors to understand the effect of an electric field to the HfO_2-based ferroelectric material properties.

2. Experimental

We analyzed carrier transport properties of HZO thin films by measuring leakage current of MFM capacitor.

Figure 1 shows a device structure of MFM capacitor and fabrication process flow. First, the bottom TaN electrode is deposited on HF-treated Si substrate by DC sputtering method. Subsequently 10 nm thick $Hf_{0.5}Zr_{0.5}O_2$ layer is deposited by RF sputtering using HfO_2 and ZrO_2 targets, followed by the top TaN electrode deposition by DC sputtering. The MFM capacitors are annealed in rapid thermal annealing by halogen lamp. The annealing temperature is tuned by tuning lamping time. Top and bottom Al electrodes for electric measurement are also deposited. Leakage current (*I–V*) and Remnant polarization (*P–V*) measurements are performed [2].

3. Results

First, ferroelectricity is checked on fabricated MFM capacitors. Figure 2 shows *P–V* characteristics of MFM capacitors annealed at 640 – 930 °C. At 640 °C of annealing temperature, the *P–V* shows anti-ferroelectricity, and changes to ferroelectricity over 840 °C annealing. In the sequence of these *P–V* measurements, first "poling" triangular pulse voltage to 3 V is applied before the voltage sweep. Figure 3 shows *I–V* characteristics of MFM capacitors annealed at 640 – 930 °C. These are the same annealing conditions as in Fig. 1, but "fresh" capacitors are measured with bias from 0 V to 5 V, which exceeds the voltage of dielectric breakdown. Over the annealing temperature of 840 °C, a kink or a discontinuity point of derivative appears in *I–V* curves.

Figure 4 shows relationship between $E^{1/2}$ and I/E where E is electric field strength. This plot is known as Poole-Frenkel (*PF*) plot and transformed from *I–V* characteristics in Fig. 3 [3]. *PF* type carrier transport behavior which is modeled by trap-assisted electron transport, is represented by linear correlation in *PF* plot. As shown in the Figure, I/E–$E^{1/2}$ characteristics can be fitted by two straight lines in both sides of "kink" voltage. Slope of linear correlation in *PF* plot corresponds to apparent dielectric constant of the material. This suggests that the apparent dielectric constant of HZO "abruptly" transforms at the kink voltage.

4. Discussion

Figure 5 is result of cyclic *I–V* measurement of MFM capacitor annealed at 840 °C. Bias-voltage sweeps from 0 V to 3 V to avoid dielectric breakdown and sweeps back to 0 V again. This sweep cycle is engaged with two times. In first voltage-up sequence, kink of *I–V* appears as reported in fig. 3 but in voltage-down sequence *I–V* characteristic shows hysteretic feature and kink vanishes. In the second cycle, the *I–V* characteristic shows no hysteresis in both voltage-up and -down. The *PF*-plot also indicates that a single straight line can be fitted after first voltage-down sequence.

Figure 6 is result of cyclic *I–V* in which bias-voltage sweeps from 0 V to 3 V, subsequently sweeps back to -3 V, and finally voltage up to 0 V. This cycle is also engaged with two times. In second cycle sequence of 0 to 3 V, the *PF*-plot can be fitted with two lines with the same slope. This suggests that apparent dielectric constant is stable over all voltage region and current difference corresponds to result of polarization switch.

From these results, in initial poling treatment, apparent

dielectric constant irreversibly changes, and after the consummation of poling, dielectric constant of HZO layer is fixed with constant over all voltage regions. This feature seems different from general poling, in which only putting random direction of polarization domain together to electric field direction and no operation for material parameter. In ferroelectricity of HZO, it has been suggested that re-distribution of oxygen vacancy plays an important role. In poling treatment of ferroelectric HZO, the effect of oxygen vacancy re-distribution should be further discussed.

5. Summary

In the first poling treatment of ferroelectric $Hf_{0.5}Zr_{0.5}O_2$, irreversible transformation of carrier transport property has been observed in *I–V* measurement of MFM capacitors. It is suggested that not only the polarization direction, but also any material parameter changes in the poling treatment of $Hf_{0.5}Zr_{0.5}O_2$, system.

Acknowledgements

This work was supported by JST Japan-Taiwan Collaboration Research Program, Grant Number JPMJKB1903; and JSPS KAKENHI, Grant Number JP20238692 and JP20271473.

References

[1] D. Zhou, et al., Appl. Phys. Lett. 103 (2013) 192904.
[2] S. Migita, et al., Jpn. J. Appl. Phys. 58 (2019) SBBA07.
[3] J. Frenkel, Physical Review 54 (1938) 647.

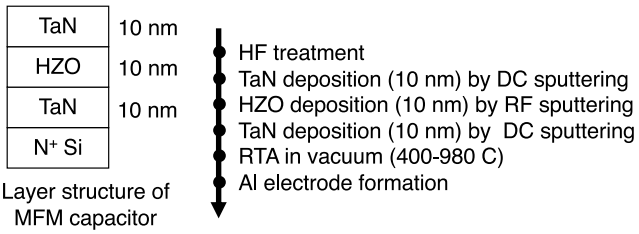

Fig. 1 Sample structure of MFM capacitor and process flow.

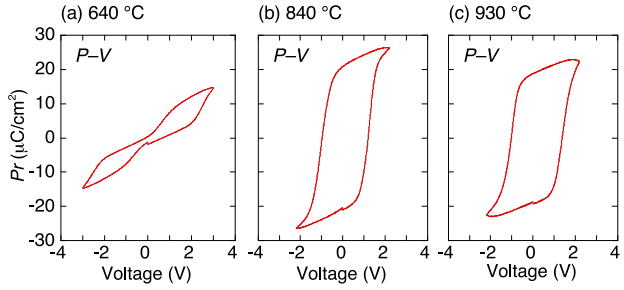

Fig. 2 *P–V* characteristics of 10 nm HZO MFM capacitors.

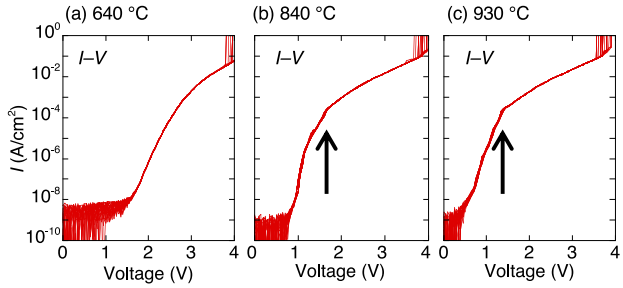

Fig. 3 *I–V* characteristics of 10 nm HZO MFM capacitors. 26 of fresh MFM capacitors are measured in each plot. Arrows in (b) and (c) show kink in *I–V* characteristics.

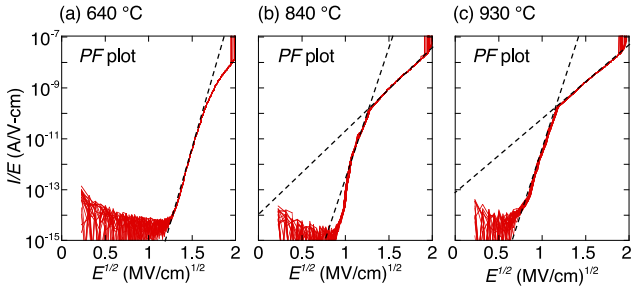

Fig. 4 *PF* plot transformed from *I–V* characteristics of Fig. 3.

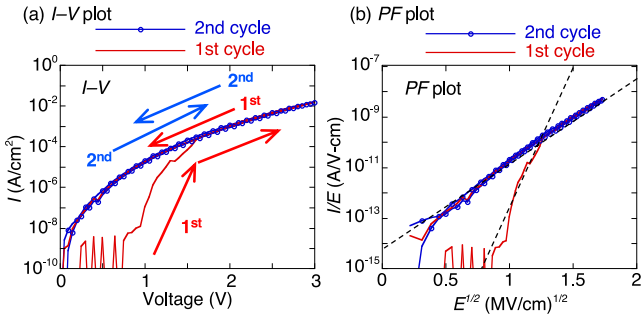

Fig. 5 Result of cyclic *I–V* measurement between 0 and +3 V. Annealing temperature of MFM capacitor is 840 °C. *PF* plot is transformed from *I–V* characteristic of (a).

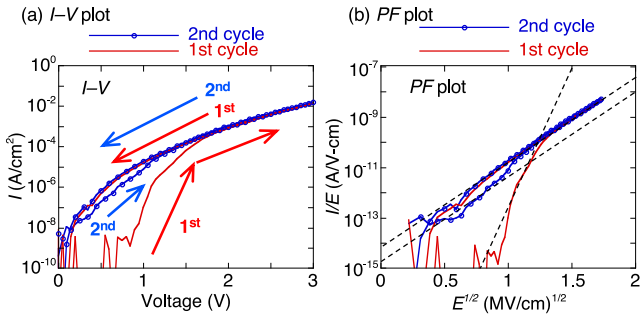

Fig. 6 Result of cyclic *I–V* measurement between -3 and +3 V. 0 to +3 V voltage region is shown. Annealing temperature of MFM capacitor is 840 °C. PF plot is transformed from *I–V* characteristic of (a).